AGU PUBLICATIONS

Geophysical Research Letters

RESEARCH LETTER
10.1002/2016GL068653

Key Points:
- Seasonal predictability of significant wave height in the Indo-Pacific Ocean is investigated
- There is potential for predicting wave height with several months lead time during boreal summers
- ENSO has a nonlinear influence on the number of extreme significant wave height events

Supporting Information:
- Supporting Information S1

Correspondence to:
H. Lopez,
hlopez@rsmas.miami.edu

Citation:
Lopez, H., and B. P. Kirtman (2016), Investigating the seasonal predictability of significant wave height in the West Pacific and Indian Oceans, *Geophys. Res. Lett.*, *43*, 3451–3458, doi:10.1002/2016GL068653.

Received 11 MAR 2016
Accepted 23 MAR 2016
Accepted article online 29 MAR 2016
Published online 6 APR 2016

Investigating the seasonal predictability of significant wave height in the West Pacific and Indian Oceans

Hosmay Lopez[1,2] and Ben P. Kirtman[3]

[1]Cooperative Institute for Marine and Atmospheric Studies, University of Miami, Coral Gables, Florida, USA, [2]Atlantic Oceanographic and Meteorological Laboratory, NOAA, Miami, Florida, USA, [3]Rosenstiel School of Marine and Atmospheric Sciences, University of Miami, Coral Gables, Florida, USA

Abstract This study investigates seasonal prediction skill of significant wave height (SWH) in the West Pacific and Indian Oceans. We forced the WAVEWATCH III model with 10 m winds from the National Centers for Environmental Prediction Reanalysis-2 and from the Community Climate System Model version 4 North American Multi-Model Ensemble retrospective forecasts for the period of January 1979 to December 2013. Results indicate potential for predicting SWH with several months lead time during boreal summers after the warm phase of El Niño–Southern Oscillation (ENSO) measured by deterministic and probabilistic skill scores in the Northwest Pacific and Bay of Bengal. During these summers, SWH is smaller than normal due to reduced atmospheric synoptic activity associated with an anomalously anticyclone in the western Pacific, leading to larger signal-to-noise ratio in the 10 m winds, hence increasing SWH prediction skill. It is shown that ENSO has a nonlinear influence on the number of extremely large SWH events, with reduced number of extreme occurrences during boreal summers after the warm phase of ENSO.

1. Introduction

Understanding the physical processes at the air-sea interface is a key in order to understand current climate and future climate projections. Processes like momentum, heat, and freshwater fluxes through the air-sea interface are main drivers of the climate system and are also affected by variability of ocean surface gravity waves [*Li and Garrett*, 1997; *Hanley and Belcher*, 2008; *Fan et al*., 2009]. In addition to modulating surface fluxes, these ocean surface gravity waves affect commerce, military operations, communications, and recreational activities in coastal areas. Recent studies have argued for the existence of trends in wave height for the last several decades [*Hemer et al*., 2010; *Izaguirre et al*., 2011]. These trends will likely influence the delicate equilibrium of coastal regions as well as present new challenges for offshore engineering infrastructures [*Weisse et al*., 2008]. Future climate projections, as reported by the Intergovernmental Panel for Climate Change, have recognized the effect of climate change on coastal regions like erosion and impact on population and ecosystem as one of the main requirements for the assessment [*Nicholls et al*., 2007].

There are several studies that describe the wind and surface wave climate [*Young*, 1999; *Woolf et al*., 2002; *Vinoth and Young*, 2011]. The latest knowledge on the current wave climate is owed to the development of phase-averaged surface wave models such as WAVEWATCH III (WW3) of *Tolman et al*. [2002] and Wave Model of *Wamdig* [1988]. Interannual wave climate variability responds to changes in large-scale ocean-atmosphere systems. The relationship between wave height and well-known climate indices has been studied. For example, *Hemer et al*. [2010] argue that wave climate variability in the Pacific Ocean is influenced by the El Niño–Southern Oscillation (ENSO). The leading mode of wave climate variability in the Southern Ocean is significantly correlated with the Southern Annular Mode [*Hemer et al*., 2010]. Similarly, *Izaguirre et al*. [2010] showed that wave height variability in the North Atlantic is related to the North Atlantic Oscillation.

All of these studies seek to understand surface ocean wave height variability and the possible climate predictors. The objective of this paper is to study whether there is a potential predictability of significant wave height (SWH) beyond the traditional synoptic weather time scale. In order to test the seasonal predictability of SWH, the WW3 model will be forced with atmospheric reanalysis winds and winds from a set of seasonal retrospective prediction experiments using the Community Climate System Model version 4 (CCSM4) from the North American Multi-Model Ensemble (NMME) Project [*Kirtman et al*., 2014] over the western Pacific and Indian Oceans. The WW3 experiment with atmospheric reanalysis forcing will be used throughout at a

proxy for observational estimates in the forecast verifications presented here. While not real observational estimates, the experiment with reanalysis forcing does provide a homogenous record for verification.

2. Wave Model and Experiment Design

The wave model used in this study is WAVEWATCH III (version 3 model). It is an operational wave model used by the National Centers for Environmental Prediction (NCEP)/Environmental Prediction Center [*Tolman*, 1998] for global and regional significant wave height forecasts. It uses realistic bathymetry from the Naval Oceanographic Office DBDB5 database. WAVEWATCH3 (WW3) uses four time steps: a global time step for propagation of the model solution and interval for wind input, a spatial time step used for spatial propagations, a spectral time step employed for interspectral propagation, and a source time step used for source terms which are dynamically adjusted for each grid point and global time step.

The wind forcing consisting of 10 m daily winds is interpolated by WW3 using a temporal linear interpolation of speed and direction. We assert that the use of daily instead of hourly winds forcing will not qualitatively alter our overarching result, although we acknowledge that this potential shortcoming is beyond the scope of this paper. The speed is corrected in order to conserve the energy input instead of the wind velocity. Spatial interpolation from input wind forcing grid to WW3 model grid is performed using a bilinear interpolation of each of the vector components, which include corrections for conserving the wind energy. Forecast of wave height from WW3 model has been validated for global and regional domains [*Tolman et al*., 2002] and was shown to overestimate wave height in the presence of extremely high winds [*Chao et al*., 2005; *Tolman et al*., 2005]. In contrast, *Fan et al*. [2012] showed a good agreement of significant wave height simulated by WW3 with respect to in situ buoys, satellite altimeter measurements, and reanalysis products, although comparing results from different studies is complicated in that they used different source functions that led to different wave height estimations.

This paper focuses on Australian and Indonesian domains (80°E–180°E and 60°S–40°N) with a grid resolution of 1°. In order to assess the predictability of significant wave height, we force WW3 model with the NCEP Reanalysis-2 daily 10 m winds for the period of January 1979 to December 2013. The NCEP Reanalysis has a spatial resolution of 1.9 [*Kistler et al*., 2001] which is interpolated to the WW3 grid resolution. The wave height obtained from this case is used for verification of the forecasts described below. We acknowledge that this simulated wave height is not an observational estimate and is not ideal; however, this approach does provide a homogenous record to evaluate the retrospective forecast skill.

Similar to the verification simulation, WW3 model is integrated using the 10 m wind as forcing from the CCSM4 NMME retrospective forecasts. CCSM4 is an earth system model consisting of atmosphere, land, ocean, glaciers, and sea ice components, all of which are linked by a flux coupler. The coupler exchanges daily information among the components interactively while the models run. The atmospheric component has 26 vertical levels with horizontal resolution of 0.9° latitude by 1.25° longitude. The ocean model component uses the Parallel Ocean Program version 2 with 1° horizontal resolution and 60 vertical levels. The CCSM4 retrospective forecasts have 10 ensemble members each with distinct initial conditions. Each member is initialized in 1 January and 1 May and integrated for 12 months for the period of 1982–2013. Overall, we have 32 forecasts years, initialized twice a year and each with 10 ensemble members for a total of 640 model years. The forcing of WW3 with CCSM4 winds will be referred to as CCSM4-WW3 model.

3. Results

Before discussing the seasonal predictability, it is necessary to assess whether CCSM4-WW3 reproduces the mean characteristics of SWH compared to that obtained from NCEP Reanalysis. For this, we assess the model fidelity for each of the four regions identified in Figure S1 in the supporting information. This is motivated because each region has a distinct SWH climate. Figure S2 (supporting information) shows a Taylor diagram of SWH for each of the four regions for all lead times. The Taylor diagram is a simple tool to represent the accuracy of one model in reproducing observed features. In the context of this paper, it describes how accurate spatial coherence of SWH is reproduced by CCSM4-WW3 compared to NCEP. We note that the model agrees well with observational estimate (i.e., simulation using NCEP reanalysis forcing) in that spatial correlation is greater than 0.85 for all regions. The bias, as measured by the RMSE error, remains less than 0.5 and remains smaller than the standard deviation (σ) for each region. Given this, the Northwest Pacific region

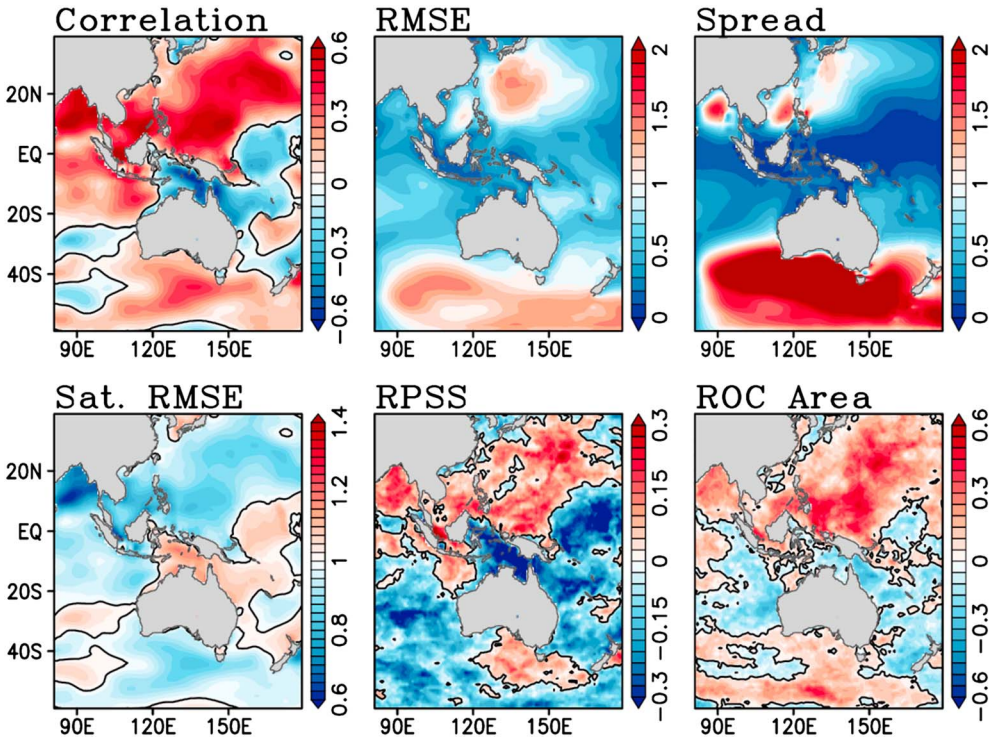

Figure 1. Significant wave height forecast skill assessment for May ICs, verified on boreal summer (i.e., June-July-August-September, JJAS). RMSE and spread have units of meters (m); all others are unitless.

(red) stands out by having smaller correlation but closer to observed variance than the other three regions, although the RMSE for this region is slightly larger than for the others.

The objective here is to quantify SWH predictability using 10 m winds from an ensemble simulation of CCSM4 as forcing of WW3 model. But we must remove systematic errors in SWH before any analysis on skill score is performed. Typically, in the "perfect model predictability framework", it is not necessary to remove the systematic error. In this case, it is because we deviate from perfect model when verifying the prediction skill of CCSM4-WW3 model against the SWH obtained from NCEP winds. The systematic error has been removed in all subsequent analysis following *Lopez and Kirtman* [2014].

Figure 1 presents several forecast verification metrics, including deterministic and probabilistic methods for lead times 3–5 months corresponding to boreal summer when the forecasts are initialized in 1 May. Anomaly correlation is considerably higher over the NW Pacific and the Bay of Bengal. Even though anomaly correlation is considered to be a good metric of prediction skill, it does not provide any information on the amplitude of the forecast error. We rely on RMSE, which shows larger values over the extratropics in both hemispheres. The region just south of Japan shows large RMSE errors even when the correlation is large. This region is also associated with large ensemble spread. A large spread should not be mistaken for a lack of skill; this depends on whether the spread is a good representation of the RMSE (i.e., a well-calibrated prediction system). Over the extratropics, the ensemble spread is larger than the RMSE, suggesting that CCSM4-WW3 is underconfident in SWH prediction. The opposite occurs near the equator, where the model is overconfident in its forecasts, which reduces reliability. Given the large spatial extent of the domain, a better measure of deterministic skill is the saturation RMSE score. This measures the forecast error relative to the system internal variability. As is evident in Figure 1, the skill over the NW Pacific and Bay of Bengal is better than for the other regions as measured by saturation RMSE. Note that SWH error saturates in the equatorial Pacific and part of the Southern Ocean. This is further shown by probabilistic measures of forecasts skill, namely, Rank Probability Skill Score (RPSS) and Relative Operating Characteristics (ROC). The RPSS measures the probabilistic skill relative to a climatological forecast; hence, an RPSS score greater than zero is said to be better than climatology. The NW Pacific region is the only one that has positive RPSS scores, consistent with deterministic measures. This is further validated by the ROC score, which measures the probabilistic skill of a

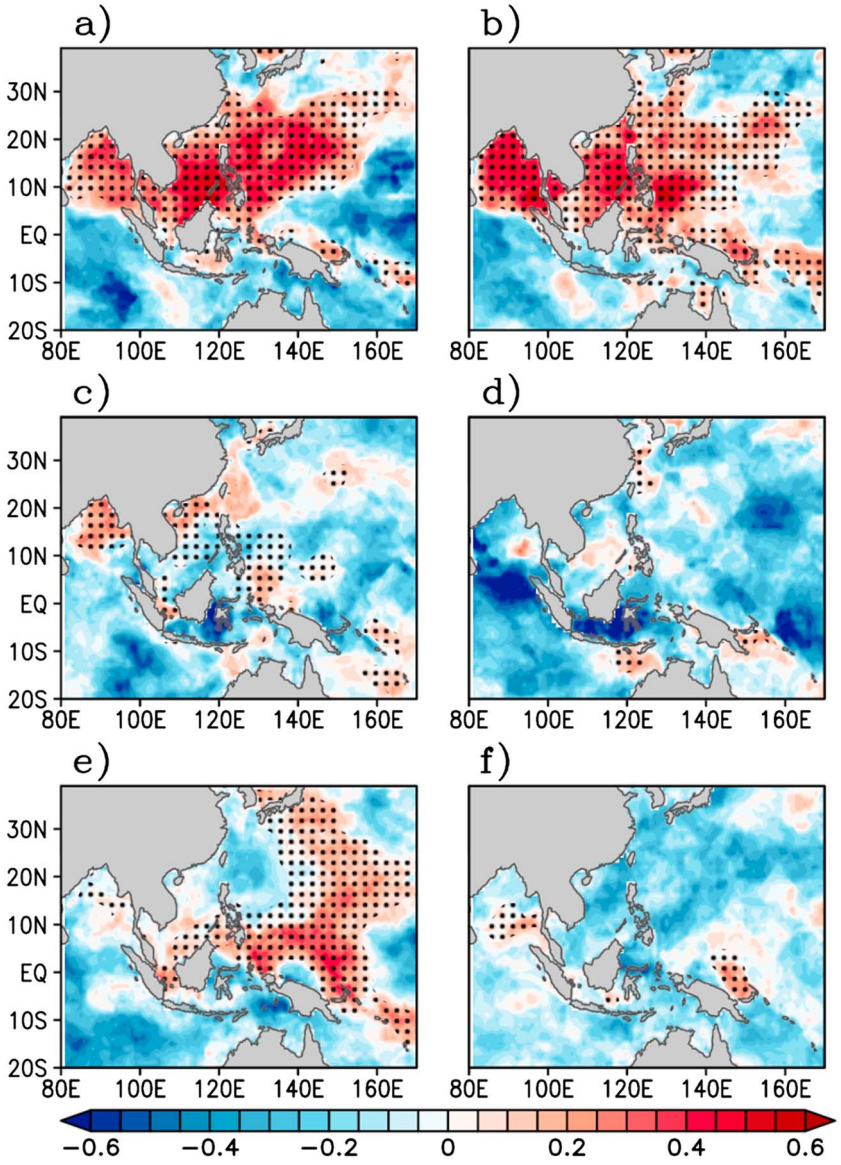

Figure 2. Relative Probabilistic Skill Score (RPSS, color) and anomaly correlation greater than 0.5 (black stipples) for significant wave height forecast verified in boreal summer (i.e., lead time 4 months for May ICs and lead time 8 months for January ICs). (a, c, and e) May ICs during El Niño, neutral, and La Niña years. (b, d, and f) January ICs. ENSO years are defined based on terciles of Niño 3 SST anomaly during December-January-February.

forecast system by comparing hit rates and false alarm rates. The hit rate indicates the proportion of events for which a warning was issued correctly, providing an estimate of the probability that an event will be forewarned. The false alarm rate is the proportion of nonevents for which a warning was issued incorrectly. Given this, a ROC score index greater than zero is said to be a skillful probabilistic forecast. In term of SWH, we define an event as the upper tercile of wave height. It is shown that the hit rate over the NW Pacific is considerably larger than the false alarm rate for these events. Deterministic and probabilistic measures of forecast skill suggest the potential for skillful seasonal forecasts of SWH in the Northwest Pacific.

Given the June-July-August-September (JJA) prediction skill noted in Figure 1, we ask what is the source of the skill? Despite the fact that ENSO peaks in the boreal winter and is comparatively weak in JJA, it remains of most obvious potential source of skill. To assess this, we analyze the skill conditioned by the state of ENSO. Here El Niño (La Niña) is identified by December-January-February (DJF) Niño 3 Sea Surface Temperature (SST) anomaly greater than one standard deviation. In total, 9 El Niño, 11 neutral, and 7 La Niña events were

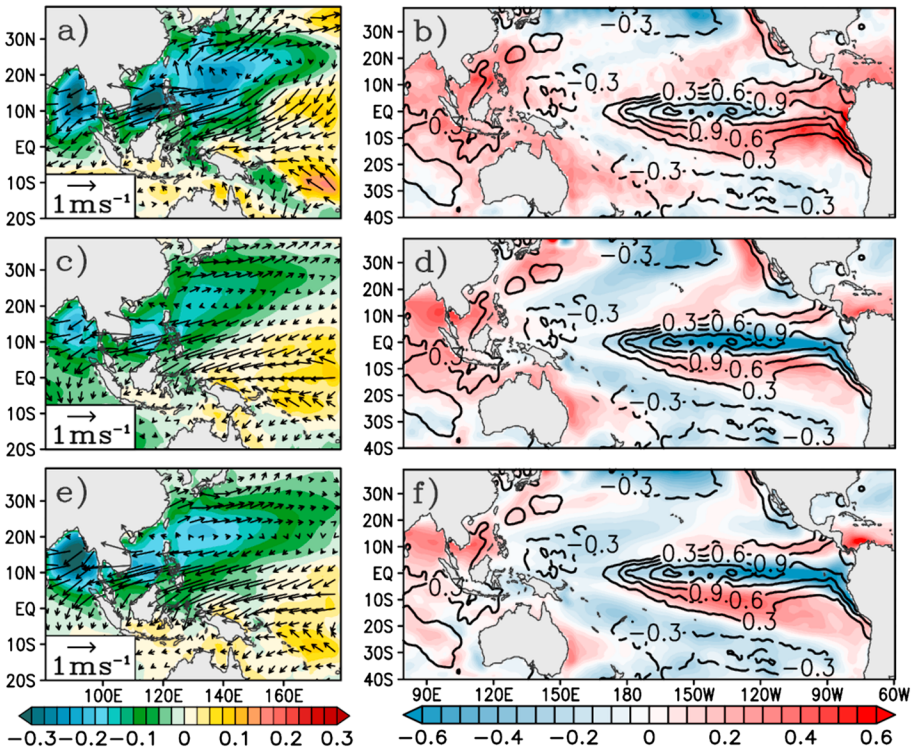

Figure 3. (a) Composite of observed boreal summer significant wave height anomaly (meters, color) and 10 m wind anomaly after peak phase of El Niño events. (b) Sea surface temperature (SST) anomaly during boreal summer (color) and peak phase of El Niño (black contour). (c and d) Same as Figures 3a and 3b but for forecast using May ICs (i.e., lead time 4 months). (e and f) Forecasts using January ICs (i.e., lead time 8 months).

considered from 1982 to 2010. The prediction skill is then quantified for June-July-August (JJA + 1) after the DJF ENSO state. The motivation for this analysis is twofold. First, there is enhance skill during boreal summer (see Figure 1), and second, there is a well-known relationship between ENSO and the NW Pacific Subtropical High [*Wang et al*., 1999, 2000; *Li et al*., 2007; *Chen et al*., 2012; *Yun et al*., 2015]. Here we also include the retrospective forecasts initialized on 1 January and 1 May both verifying in boreal summer. Therefore, in this assessment we are examining whether there is prediction skill 7–9 months in advance in the January cases and one season in advance in the May case. Figure 2 shows the RPSS (color) and anomaly correlation greater than 0.5 (black stipples) for SWH forecast verified in boreal summer (i.e., lead time 4 months for May initial conditions (ICs) and lead time 8 months for January ICs). Figures 2a, 2c, and 2e are for May ICs during El Niño, neutral, and La Niña years. Similarly, Figures 2b, 2d, and 2f are for January ICs. It is evident that most of the forecast skill over the Northwest Pacific discussed earlier can be attributed to the warm phase of ENSO and that there is only a relatively small degradation in forecast skill as lead time increases (Figures 2a and 2b). In contrast, those summers that follow neutral- or La Niña-type conditions in the tropical Pacific offer little or no forecast skill, although for the latter there is some skill for SWH predictions in the tropical western Pacific when the forecasts are initialized on 1 May (Figure 2e).

How does the warm phase of ENSO modulate predictability of significant wave height? In an attempt to answer this question, Figure 3 shows the composite of boreal summer SWH anomaly (color) and 10 m winds (vector) after the peak phase of El Niño events for (a) NCEP simulated, (c) forecasts initialized on 1 May (i.e., lead time 4 months), and (e) forecasts initialized on 1 January (lead time 8 months). The NCEP simulation suggests negative SWH anomaly over the NW Pacific and Bay of Bengal in the boreal summers after the peak phase of the El Niño events (Figure 3a). This negative anomaly is reasonably well captured by the forecasts initialized in May (Figure 3c) for short lead time and January (Figure 3e) for long leads. It is also shown that CCSM4-WW3 captures the anomalous anticyclone [*Wang et al*., 1999] which enhances easterlies from the equator to 15°N and westerlies north of 25°N. This anomalous circulation pattern is indicative of a strengthening of the West Pacific subtropical high. This is consistent with *Yun et al*, [2015], which showed that El Niño

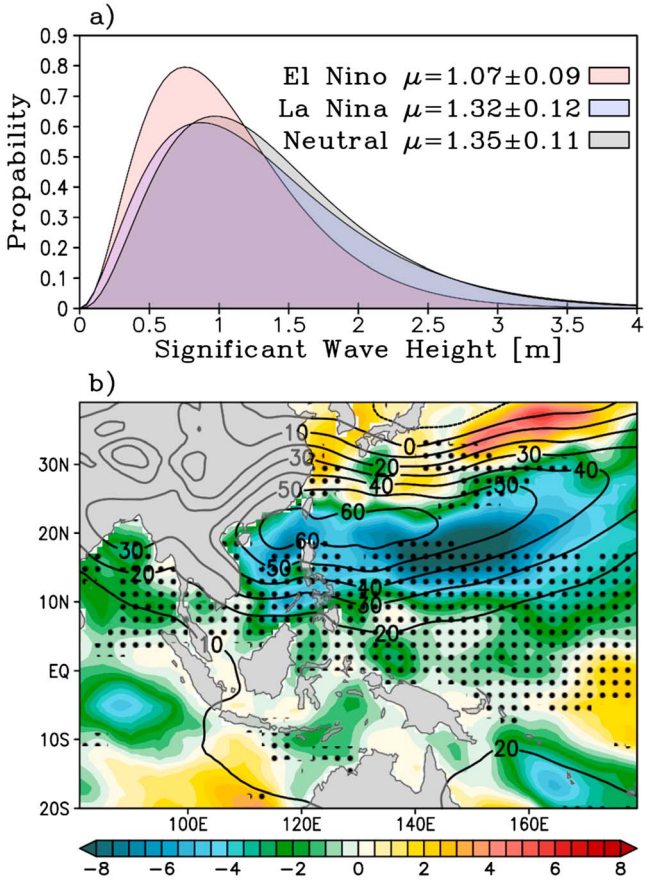

Figure 4. (a) Significant wave height probability density function (PDF) for the Northwestern Pacific region during JJA (+1) for each ENSO phase. The legend shows the mean (μ) wave height and its 99% confidence interval. (b) Composite difference during El Niño minus neutral years of 10 m eddy kinetic energy (EKE, color). EKE is calculated as the sum of the squared zonal and meridional 10 m wind anomalies, where anomalies are defined by removing the monthly mean from the daily wind components. Also shown is the regression of 850 mb geopotential height with Niño 3 SST index (black contour). Black stipples denote regions where JJA (+1) signal-to-noise ratio of both the zonal and meridional 10 m winds during El Niño is larger than those during neutral conditions.

tends to intensify the subtropical high from spring to summer. We suggest that during boreal summers following the peak phase of an El Niño event, the West Pacific subtropical high strengthens, influencing SWH in that region. The CCSM4-WW3 prediction system is able to capture elements of this feature irrespective of lead time. This is somewhat surprising given the relatively weak amplitude of ENSO during the boreal summer as shown in Figures 4b, 4d, and 4f for observed, forecasts initialized in May, and forecasts initialized in January, respectively.

As further evidence for the influence of the warm phase of ENSO, Figure 4a shows the probability density function (PDF) of SWH for the NW Pacific region during boreal summers conditioned by the ENSO state of the previous DJF season. First, we note that SWH follows a Gamma distribution with significant right skewness. Note that the PDF during La Niña and neutral conditions is statistically undistinguishable. In contrast, consistent with Figure 3, there is significant wave height reduction during those summers that follow El Niño events. The reduction in SWH during summers following the peak phase of El Niño and the asymmetric prediction skill can be attributed to a reduction in 10 m eddy kinetic energy (EKE) shown in Figure 4b (color). Here EKE includes synoptic and other high-frequency atmospheric variability that typically would serve to reduce the signal-to-noise ratio (SNR). This reduced EKE activity during El Niño is attributed to the strengthening of the West Pacific subtropical high (black contour), which serves to block midlatitude synoptic weather features like cold surges and transient eddies. This is evident by the anomalous positive EKE in the northern flanks of the anomalous subtropical height where atmospheric eddy activity is enhanced and thus reduces SWH prediction skill there. To further validate this, Figure 4b depicts the composite difference (i.e., El Niño minus neutral condition) of SNR of 10 m wind (black stipples). The larger SNR for most of the region during El Niño events is readily seen. A higher SNR of 10 m wind is a good indication of higher potential predictability of SWH, given that 10 m wind is the only forcing applied to CCSM4-WW3 forecasting system.

4. Extreme Value Theory and Wave Height

Thus far, we have looked at the prediction skill of SWH and how it is influenced by ENSO state. Most notably, there is significant change in the PDF of SWH during the warm phase of ENSO. Motivated by this result, we explore in more detail of the influence of ENSO on extreme SWH events by analyzing the right tail of the SWH distribution. Extreme value theory is a statistical technique that describes the unusual rather than the usual events. Here a peak-over-threshold method using the Generalized Pareto (GP) distribution

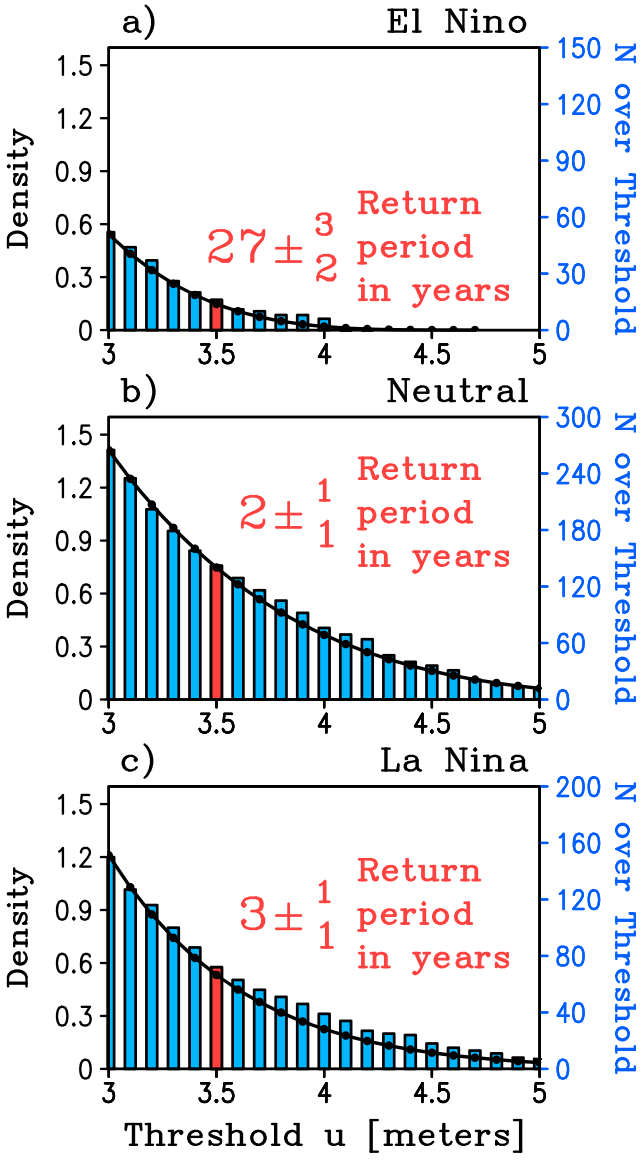

Figure 5. Generalized Pareto Distribution (black line) and number of days *N* above high threshold *u* of JJA significant wave height for (a) El Niño, (b) neutral, and (c) La Niña years. Return period (in years) for the 3.5 m wave height is shown in red plus/minus error at a 95% confidence level.

[*Coles*, 2001] is used. We model the excess over a high threshold by looking at JJA daily mean SWH greater than a fixed threshold. The Generalized Pareto (GP) cumulative density function with shape a, scale σ, and threshold u parameters is as follows:

$$\mathrm{CDF}(x,a,\sigma,u) = 1 - \left[1 + a\frac{x-u}{\sigma}\right]^{-1/a}, \quad (1)$$

$$x > u, a\frac{x-u}{\sigma} > -1$$

The excess over a threshold u corresponds to daily SWH exceeding the high threshold u. A large range of u is chosen to test the sensitivity of the results. We only kept those values of u for which the estimate of the shape and scale parameters were stable, based on a parameter variance analysis. In order to avoid correlation between supposedly independent values for a given location, we cluster excess over threshold u by identifying independent clusters and keeping only one value per cluster. Each cluster must be separated from the rest by at least 8 days, which guaranties that each extreme is synoptically independent. Given the rareness of extreme events and the relative few ENSO events from 1982 to 2013, all ensemble members for both initial conditions are used in order to increase sample size.

The GP distribution is shown in Figure 5 (black line) for boreal summer SWH preceded by (a) El Niño with threshold parameter u equal to 2.3 m, (b) neutral with u equal to 3 m, and (c) La Niña with u equal to 2.9 m. Figure 5 also shows the number of days N that the threshold is exceeded (blue bars). There is a considerable change in the distribution of extreme SWH events conditioned by the state of the tropical Pacific SST, with extreme high SWH events being more likely during neutral and La Niña conditions. The modeled GP distribution is a good fit of the observed threshold exceeded. Note that the occurrence of SWH extremes greater than 3.5 m is very rare during summers preceded by El Niño, with return period of 27 years. In contrast, these extremes occur every 2 years for summers proceeded by neutral and 3 years for La Niña conditions. Overall, SWH prediction skills along with its mean and extreme value distributions are modulated by the warm phase of ENSO.

5. Discussion

A prediction skill assessment of significant wave height over the Indo-Pacific region was performed. The output of the NMME CCSM4 retrospective forecasts was used as initial conditions and forcing for WW3 to assess whether there is a potential for multiseasonal prediction of SWH. The results indicate that there is the potential for predicting SWH with several months lead time depending on underlying ocean state. During the boreal

summer following the peak phase of El Niño there is notable predictability of SWH in the NW Pacific and the Bay of Bengal. This result is particularly noteworthy since the amplitude of ENSO during boreal summer is quite weak. It is worth noting that the results are consistent whether the two extreme El Niño events of 1982–83 and 1997–98 are excluded/included in the analysis (Figure S6, supporting information). During boreal summer the wave height is smaller than normal as a result of reduced atmospheric synoptic activity associated with an anomalous anticyclone [*Wang et al*., 1999] which strengthens the West Pacific subtropical high. This leads to a larger signal-to-noise ratio in the 10 m winds, hence increasing significant wave height predictability. This relationship between the strength of the West Pacific subtropical high and ENSO was studied in *Yun et al*. [2015] who showed that El Niño tends to intensify the subtropical high from spring to summer, thus leading to the decay of the ENSO event via easterly wind modulation. Consequently, this allows for prediction skill of SWH with several seasons lead time. This nonlinear influence of ENSO on SWH was further demonstrated by an extreme value analysis. It was shown that the number of extremely large SWH events was significantly reduced during boreal summer preceded by the warm phase of ENSO. We also tested whether the results presented here are affected by the limited domain size used. A parallel experiment was carried out using a global domain for WW3 to check the influence of remotely forced swells on SWH predictability. We found that the root-mean-square difference (regional-global simulations) is less than 0.2, which is significantly smaller than the RMSE of the forecasts of about 0.6 (Figure 1). The correlation between the regional and global WW3 model runs is greater than 0.95; this is considerably larger than the forecast correlation. This suggests significant agreement between the SWH obtained from the regional and global model simulations (see supporting information).

Acknowledgments
We would like to acknowledge the three anonymous reviewers for their insightful comments. Data can be obtained upon request by contacting the corresponding author at hlopez@rsmas.miami.edu. The authors acknowledge support from ONR award N000141310439 and NOAA awards NA15OAR4320064 and NA12OAR4310089.

References

Chao, Y. Y., J. H. G. M. Alves, and H. L. Tolman (2005), An operational system for predicting hurricane-generated wind waves in the North Atlantic Ocean, *Weather Forecasting*, *20*, 652–671.

Chen, W., J.-K. Park, B. Dong, R. Lu, and W.-S. Jung (2012), The relationship between El Niño and the western North Pacific summer climate in a coupled GCM: Role of the transition of El Niño decaying phases, *J. Geophys. Res.*, *117*, D12111, doi:10.1029/2011JD017385.

Coles, S. (2001), *An Introduction to Statistical Modeling of Extreme Values*, Springer, London.

Fan, Y., I. Ginis, and T. Hara (2009), The effect of wind–wave–current interaction on air–sea momentum fluxes and ocean response in hurricanes, *J. Phys. Oceanogr.*, *39*, 1019–1034.

Fan, Y., S.-J. Lin, I. M. Held, Z. Yu, and H. L. Tolman (2012), Global ocean surface wave simulation using a coupled atmosphere-wave model, *J. Clim.*, *25*(18), 6233–6252.

Hanley, K. E., and S. E. Belcher (2008), Wave-driven wind jets in the marine atmospheric boundary layer, *J. Atmos. Sci.*, *65*, 2646–2660.

Hemer, M. A., J. A. Church, and J. R. Hunter (2010), Variability and trends in the directional wave climate of the Southern Hemisphere, *Int. J. Climatol.*, *30*, 475–491.

Izaguirre, C., F. J. Mendez, M. Menendez, A. Luceño, and I. J. Losada (2010), Extreme wave climate variability in southern Europe using satellite data, *J. Geophys. Res.*, *115*, C04009, doi:10.1029/2009JC005802.

Izaguirre, C., F. J. Mendez, M. Menendez, and I. J. Losada (2011), Global extreme wave height variability based on satellite data, *Geophys. Res. Lett.*, *38*, L10607, doi:10.1029/2011GL047302.

Kirtman, B. P., D. Min, J. M. Infanti, J. L. Kinter III, D. A. Paolino, Q. Zhang, H. van den Dool, S. Saha, M. P. Mendez, and E. Becker (2014), The North American Multi-Model Ensemble (NMME): Phase-1 seasonal to interannual prediction; Phase-2 toward developing intra-seasonal prediction, *Bull. Am. Meteorol. Soc.*, *95*(4), 585–601, doi:10.1175/BAMS-D-12-00050.1.

Kistler, R., *et al*. (2001), The NCEP-NCAR 50-year reanalysis: Monthly means CD-ROM and documentation, *Bull. Am. Meteorol. Soc.*, *82*(2), 247–267.

Li, M., and C. Garrett (1997), Mixed-layer deepening due to Langmuir circulation, *J. Phys. Oceanogr.*, *27*, 121–132.

Li, Y., R. Lu, and B. Dong (2007), The ENSO-Asian monsoon interaction in a coupled Ocean–Atmosphere GCM, *J. Clim.*, *20*, 5164–5177.

Lopez, H., and B. P. Kirtman (2014), WWBs, ENSO predictability, the spring barrier and extreme events, *J. Geophys. Res. Atmos.*, *119*, 10–114.

Nicholls, R. J., P. P. Wong, V. R. Burkett, J. O. Codignotto, J. E. Hay, R. F. McLean, S. Ragoonaden, and C. D. Woodroffe (2007), Coastal systems and low-lying areas, in *Climate Change 2007: Impacts, Adaptation and Vulnerability*, edited by M. L. Parry et al., pp. 315–356, Cambridge Univ. Press, Cambridge, U. K.

Tolman, H. L. (1998), Validation of a new global wave forecast system at NCEP, in *Ocean Wave Measurements and Analysis*, edited by B. L. Edge and J. M. Helmsley, pp. 777–786, ASCE.

Tolman, H. L., and J. H. G. M. Alves (2005), Numerical modeling of wind waves generated by tropical cyclones using moving grids, *Ocean Modell.*, *9*, 305–323.

Tolman, H. L., B. Balasubramaniyan, L. D. Burroughs, D. V. Chalikov, Y. Y. Chao, H. S. Chen, and V. M. Gerald (2002), Development and implementation of wind generated ocean surface wave models at NCEP, *Weather Forecast.*, *17*(2), 311–333.

Vinoth, J., and I. R. Young (2011), Global estimates of extreme wind speed and wave height, *J. Clim.*, *24*(6), 1647–1665.

WAMDIG (1988), The WAM model—A third generation ocean wave prediction model, *J. Phys. Oceanogr.*, *18*(12), 1775–1810.

Wang, C., R. H. Weisberg, and J. Virmani (1999), Western Pacific interannual variability associated with the El Niño–Southern Oscillation, *J. Geophys. Res.*, *104*, 5131–5149, doi:10.1029/1998JC900090.

Weisse, R., *et al*. (2008), Regional meteo-marine reanalyses and climate change projections: Results for Northern Europe and potentials for coastal and offshore applications, *Bull. Am. Meteorol. Soc.*

Woolf, D. K., P. G. Challenor, and P. D. Cotton (2002), Variability and predictability of the North Atlantic wave climate, *J. Geophys. Res.*, *107*(C10), 3145, doi:10.1029/2001JC001124.

Young, I. R. (1999), Seasonal variability of the global ocean wind and wave climate, *Int. J. Climatol.*, *19*, 931–950.

Yun, K. S., K. J. Ha, S. W. Yeh, B. Wang, and B. Xiang (2015), Critical role of boreal summer North Pacific subtropical highs in ENSO transition, *Clim. Dyn.*, *44*(7–8), 1979–1992.